

A multimodality vascular imaging phantom with fiducial markers visible in DSA, CTA, MRA, and ultrasound

Guy Cloutier^{a)}

Laboratory of Biorheology and Medical Ultrasonics, Research Center, University of Montreal Hospital, Montréal, Québec H2L 2W5, Canada

Gilles Soulez and Salah D. Qanadli^{b)}

Department of Radiology, University of Montreal Hospital, Québec, Canada

Pierre Teppaz

Laboratory of Biomedical Engineering, Clinical Research Institute of Montreal, Québec, Canada

Louise Allard and Zhao Qin

Laboratory of Biorheology and Medical Ultrasonics, Research Center, University of Montreal Hospital, Montréal, Québec H2L 2W5, Canada

François Cloutier

F. C. Conception, Trois-Rivières, Québec, Canada

Louis-Gilles Durand

Laboratory of Biomedical Engineering, Clinical Research Institute of Montreal, Québec, Canada

(Received 24 November 2003; revised 11 March 2004; accepted for publication 22 March 2004; published 24 May 2004)

The objective was to design a vascular phantom compatible with digital subtraction angiography, computerized tomography angiography, ultrasound and magnetic resonance angiography (MRA). Fiducial markers were implanted at precise known locations in the phantom to facilitate identification and orientation of plane views from three-dimensional (3-D) reconstructed images. A vascular conduit connected to tubing at the extremities of the phantom ran through an agar-based gel filling it. A vessel wall in latex was included around the conduit to avoid diffusion of contrast agents. Using a lost-material casting technique based on a low melting point metal, geometries of pathological vessels were modeled. During the experimental testing, fiducial markers were detectable in all modalities without distortion. No leak of gadolinium through the vascular wall was observed on MRA after 5 hours. Moreover, no significant deformation of the vascular conduit was noted during the fabrication process (confirmed by microtome slicing along the vessel). The potential use of the phantom for calibration, rescaling, and fusion of 3-D images obtained from the different modalities as well as its use for the evaluation of intra- and inter-modality comparative studies of imaging systems are discussed. In conclusion, the vascular phantom can allow accurate calibration of radiological imaging devices based on x-ray, magnetic resonance and ultrasound and quantitative comparisons of the geometric accuracy of the vessel lumen obtained with each of these methods on a given well defined 3-D geometry. © 2004 American Association of Physicists in Medicine. [DOI: 10.1118/1.1739300]

Key words: vascular phantom, vascular stenoses, ultrasonography, magnetic resonance imaging, computerized tomography, x-ray angiography, medical imaging, image calibration, fiducial markers

I. INTRODUCTION

Digital subtraction angiography (DSA), computerized tomography angiography (CTA), ultrasonography (US) and magnetic resonance angiography (MRA) are commonly used to detect and investigate the severity of vascular diseases including stenoses, thromboses, development of collateral vessels, aneurysms, or vascular malformations. Even after calibration, no imaging technique is error free. Even if CTA, especially with multi-slice isotropic imaging platforms, is considered the technique with the best 3-D spatial resolution and lowest image distortion,¹ plane x-ray angiography is still considered as a gold standard for clinical studies evaluating arterial diseases.² However, image distortion in angiography is a concern.³ For ultrasound, assumptions on the mecha-

nisms of wave propagation in biological tissues are required to reconstruct the images, and acoustic inhomogeneities of tissues can also lead to geometric distortions.⁴ The sources of image artifacts for MRA include geometric distortions due to the nonhomogeneity of the scanner fields, and magnetic interactions with the imaged object. This is why comparative studies of 3-D imaging techniques, under the same experimental conditions, are necessary to assess the accuracy and determine the advantages and limitations of each method.

Multimodality vascular flow phantoms are ideal tools as they provide a way of testing the geometric accuracy, with easy reproducibility of the experimental conditions, when different modalities are considered. They can also be used to compare the blood flow velocity patterns obtained by ultra-

sound and magnetic resonance imaging. Ideally, multimodality phantoms have to meet three major requirements. First, they must be compatible with all imaging modalities evaluated, i.e., it is important that the materials involved in the construction of phantoms allow clearly the identification of the shape of the vessel lumen on the images, with no or minimum artifacts. Second, they should be anthropomorphic, i.e., their geometry should mimic as close as possible the complexity of real human vessels. Finally, they should contain markers visible in all modalities for image calibration, rescaling and fusion.

Several compounds were used to prepare tissue-mimicking phantoms.^{5–10} Burlew *et al.*⁵ proposed a mixture of agar, graphite particles, distilled water and *n*-propanol. Others^{7,8} developed a variation of this formulation by using glycerol instead of *n*-propanol to increase the acoustic velocity of the tissue-mimic, and cellulose scattering particles instead of graphite to provide the desired acoustic attenuation. Fatty and other materials like evaporated milk-based or safflower oil with kerosene⁹ and tofu¹⁰ have also been used. As discussed later, the properties of those different tissue-mimic materials can influence the visualization of fiducial markers in multimodality imaging systems.

A. Existing vascular phantoms

Several approaches have been proposed to create realistic vascular phantoms, namely stereolithography, the casting of real vessels and lost-material methods. Stereolithography was used to build 3-D replicas of coronary and cerebrovascular vessels with stenoses.^{11–13} Until recently, this method allowed only fabricating rigid-wall phantoms with an irregular lumen surface.¹³ However, with recent developments in technologies and materials, rapid prototyping technology and stereolithography now offer an increased geometric flexibility and a better accuracy in the production of realistic three-dimensional flexible models.^{14,15} Studies were also performed on phantoms derived from real vessels harvested on cadavers.^{16–18} However, the geometry of each artery is unique and unknown, and they cannot be duplicated if the vessel is damaged. The casting of wax or cerrolow is interesting to reproduce realistic vessels with a smooth inner surface.^{6,13,19,20} The lost casting material (e.g., cerrolow) is usually filled in a two-part mold and thermally removed to create the vessel lumen. Geometries of the human carotid bifurcation and cranial blood vessels were produced with this method.

B. Use of fiducial markers

Fiducial markers are very useful in the identification and orientation of plane views in DSA, CTA, MRA and US. They can also be used for calibration, rescaling and fusion of 3-D images obtained from these different modalities, and 3-D-image reconstruction from angiographic plane views. To our knowledge, only two vascular phantoms provided fiducial markers. Frayne *et al.*⁶ used three distinct sets of lead-cored nylon fishing line as fiducial markers. However, even if the markers were visible in the projection radiography, they were

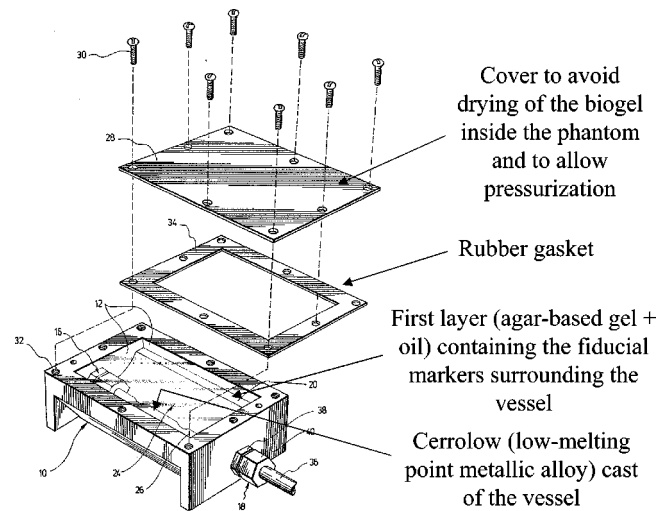


FIG. 1. Exploded perspective view of the vascular phantom before filling the box with an agar-mimicking tissue.

hardly identifiable or visible on the other image modalities. In Dabrowski *et al.*,¹⁷ eight stainless steel ball bearings pushed into an agar gel with a syringe needle were used as fiducial markers. However, ball bearings introduced artifacts in both US and CTA images. Consequently, they suggested using as few fiducial markers as possible and to reduce the ball diameter (as small as 0.119 cm) to reduce artifacts in CTA. However, small balls could not be easily detected in US images. Although not originally proposed as markers for vascular phantoms, Hill²¹ developed external markers attached to the skin that could be used for multimodality imaging (PET, MRA and CTA). These markers comprised a spherical silicone rubber void that could be filled with fluids chosen so that the markers appeared with high contrast on the images. However, the marker fluids were absorbed into the rubber over a period of a few days. Consequently, markers had to be used within 36 hours of being filled.

C. Objectives of the study

It appears from the above review that there is still a need for a multimodality vascular phantom being able to calibrate different radiology imaging apparatuses. Our goal in this study was thus to create a new phantom compatible with all vascular imaging modalities with markers visible in DSA, CTA, MRA and US. As performed by others,⁶ the vessel lumen was surrounded by a tissue-mimicking material reproducing realistic image patterns in CTA, MRA and US. Another interesting aspect was the design of an artificial vessel wall providing no image interference and avoiding the diffusion of contrast materials. The diffusion of gadolinium or other contrast agents through tissue-mimicking materials can be a concern for phantom design.²²

II. METHODS

A. Process for manufacturing the vascular phantom

As illustrated in Fig. 1, the vascular phantom was enclosed in a polyethylene container, the inner of it having a

semi-cylindrical shape surrounding the vessel lumen. The diameter of the semi-cylindrical cavity was 101.6 mm and its length was 228.6 mm. In the container, a first semi-cylindrical layer of an agar–oil mixture of controlled thickness contained a series of glass balls of 3-mm diameter. The rest of the container was filled with a block of agar-based gel (not shown in Fig. 1) with a semi-cylindrical shape at the bottom superimposed on the first layer of the agar–oil mixture. The second layer of agar gel filled the box up to the cover consisting of a polyethylene sheet. To avoid drying out of the agar-based gel and to seal the phantom during pressurization of the lumen, a rubber gasket was installed between the cover and the container. A thin layer of water was introduced between the second layer of agar and the polyethylene cover to ensure continuous acoustic coupling for ultrasound measurements.

The vascular canal ran through the second layer of agar and was connected to rigid tubing at both extremities. Garolite tubing going through the end walls of the container were used. They had the same inner diameter as that of the arterial canal, thus ensuring a smooth geometric transition between the lumen and the external tubing. Garolite is a material made of a continuous-woven glass fabric laminated with an epoxy resin. They were inserted in polypropylene bulkhead unions screwed in the end walls of the container. The rigid tubing at the extremities of the phantom provide a means of connecting the vessel to external devices such as a pump to generate fluid circulation inside the phantom, if required.

B. Composition of the two layers of gel and positioning of the markers

For the first layer, a mixture of agar–oil gel was prepared by using a volume V of a mixture containing 3 weight percent of agar and 97 weight percent water. Then a volume $V/3$ (33%) of paraffin oil (petroleum distilled solvent dewaxed paraffin, Fisher Scientific, Fairlawn, NJ, #01-184-150B) was added. The mixture was heated and energetically stirred until the gel–oil emulsion became stable, i.e., water and oil did not separate after stirring. The gel was poured into the phantom by using a special template to obtain a thickness of 4.8 mm. Time was allowed for the solidification of the gel before inserting the glass balls (fiducial markers).

As shown in Fig. 2, twenty-five geometrical fiducial markers were implanted at precise known positions in the first layer of agar–oil gel, i.e., at controlled angular positions and a depth of 3 mm from the upper cylindrical surface of the layer. They were divided in five sets of five markers each. For each set, the five balls were contained in cross-sectional and longitudinal planes of the phantom. One set was placed in the central axis, and the two sets on both sides were placed at nonsymmetrical locations to facilitate image localization. For the same reason, in each cross-sectional planar set, the balls were implanted at nonsymmetrical positions on either side of the symmetry axis.

A template was designed to position the glass balls within the first layer of agar–oil gel (see Fig. 3). The template was fixed on the top of the phantom. From the upper view, one

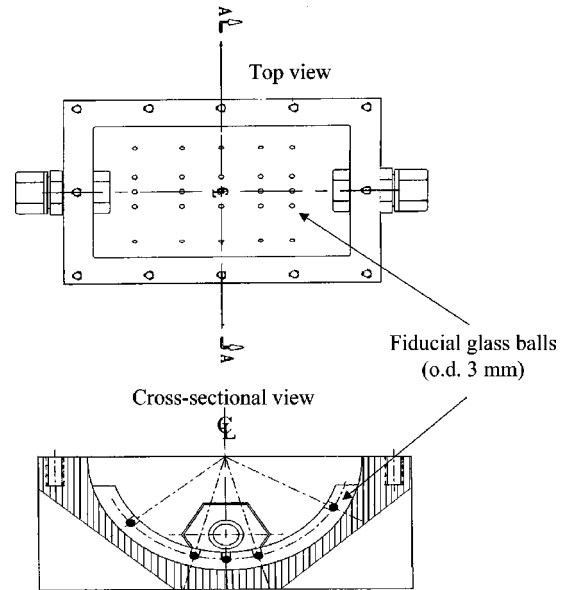


FIG. 2. Schematic of the top and cross-sectional views of the vascular phantom showing the positioning of the fiducial makers (outside diameter, o.d. = 3 mm) within the first layer of agar–oil gel.

can see four holes to fill the liquid mixture of agar–oil, and a semi-cylindrical cavity containing removable screws. The bottom part of the template was also semi-cylindrical and once it was fixed over the phantom, it allowed pouring the bottom half of the circular first layer of gel. It contained 25 removable pins, all of the same diameter (3 mm), jutting 3 mm out of the semi-cylindrical surface. These pins were used to ensure precise positioning of the fiducial markers in the

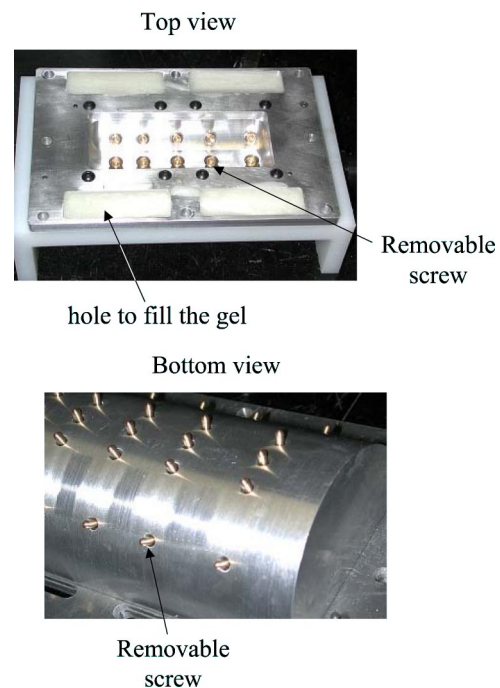


FIG. 3. Top and bottom views of the template used to pour the bottom half of the first layer of agar–oil gel. Removable screws were used to create holes allowing the positioning of the fiducial glass ball markers.

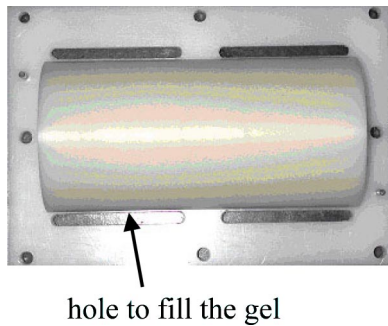


FIG. 4. The bottom view of the second template used to pour the upper half of the first layer of agar–oil gel mixture.

phantom gel. The template was designed such that the space between it and the phantom inner surface had a constant thickness. Two alignment pins on the template and corresponding holes on the top of the phantom container ensured a correct positioning. After a 3 hour solidification of the gel, the pins were unscrewed and the template removed. The glass balls were manually implanted in the holes created after removal of the pins and template. The elasticity of the gel allowed easy insertion of the balls.

A second semi-cylindrical 3.2 mm-thick layer of agar–oil gel mixture (upper half) was poured to cover the markers and fill the holes. As for the first bottom half layer, a second semi-cylindrical template (shown in Fig. 4) was used to obtain a circular layer of the required thickness. The agar–oil layer was allowed to solidify for another three hours. After solidification, the two layers of the agar–oil gel could not be distinguished from one another, both visually and on the acquired images obtained from all radiographic imaging modalities.

As reported by others,⁷ the tissue-mimicking gel mixture surrounding the vascular conduit shown in Fig. 1 was composed of 3 weight percent of agar, 8 weight percent of glycerol, 3 weight percent of cellulose particles and 86 weight percent of water. Glycerol was added to the mixture to increase the acoustic velocity of the gel, so that it became close to the value in living tissues (1540 m/s). The cellulose particles (Sigmacell, Sigma Chemical, St. Louis, MO, #S-5504) were added as an ultrasound scattering agent to provide better contrast between the vessel and the surrounding gel in B-mode ultrasonic imaging. This mixture also allowed us to mimic tissue contrast in CTA and MRA. In a first step, agar, glycerol and water were mixed together. The resulting mixture was stirred and heated until the agar powder was completely dissolved and a clear gelling liquid was obtained. Then, cellulose was added, the mixture was stirred again and cooled down to the proper temperature for pouring into the phantom, i.e., 45 °C.

C. Design of the vascular wall and lumen

The lost-material casting technique, based on the cerrowalloy and appropriate molding, can allow fabricating vascular pathologies with no axis of symmetry. To demonstrate the feasibility of the current phantom for multimodality 3-D im-

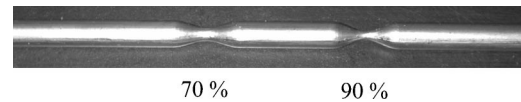


FIG. 5. A cerrowalloy piece used to mimic a vessel with a double stenosis geometry of 70% and 90% area reductions.

aging of a vessel with fiducial markers, a simple axis-symmetrical double stenoses model was designed. The stenoses had area reduction grades of 90% and 70%. The diameter of the nonobstructed part of the artery was 7.9 mm. A 58 °C melting point cerro-indium alloy core (cerrowalloy 136, Cerrometal Products, Bellefonte, PA, USA) was cast in a two-part aluminum preheated mold designed to reproduce the shape of the artery. After casting, the metallic core was cooled at room temperature for two hours. It was then extracted from the mold and hand-polished to remove surface irregularities (see Fig. 5). To avoid the diffusion of contrast materials, a thin layer of liquid latex was uniformly sprayed onto the surface of the cerrowalloy core. Time was allowed for the drying of latex.

The covered cerrowalloy positive arterial core was then installed in the phantom container. It was positioned above the circular poured agar–oil gel layer shown in Fig. 2, and it was supported at both ends of the phantom by the garolite tubes in which its extremities were inserted. The phantom was then covered by the rubber gasket and polyethylene sheet shown in Fig. 1, and positioned vertically. A small hole was made in the corner of the polyethylene sheet from which the remaining space in the phantom container was completely filled with liquid agar gel (second layer). The gel was poured at 45 °C. This temperature was found to be a good compromise because it is high enough to allow pouring before solidifying, and it is sufficiently low, compared to the melting point of cerrowalloy 136, to avoid softening and deformation of the arterial-shaped core. The vertical positioning of the phantom also allowed us to eliminate possible binding of the cerrowalloy bar due to gravity. This was required because the cerrowalloy bar is losing its rigidity following the pouring of agar. The agar gel was allowed to solidify at room temperature for approximately 10 hours. Distilled water was then added to fill the space between the solidified agar and the polyethylene sheet before closing the small hole through it with a rubber plug.

To create the vessel lumen, the vertically oriented phantom was heated in a water bath at 65 °C for 2 to 3 hours. As the temperature inside the phantom reached 58 °C, cerrowalloy started melting out of the phantom via the garolite tubes. Removal of the molten cerrowalloy created in the gel a conduit with a latex wall having the shape of the initial cerrowalloy cast. Small residual cerrowalloy particles were removed by injection of hot water in the conduit with a syringe.

D. Tissue-mimic ultrasound properties

The acoustic properties (velocity, attenuation, scattering) of agar-based gel made of glycerol and cellulose particles (the second layer of the phantom) are well described in the

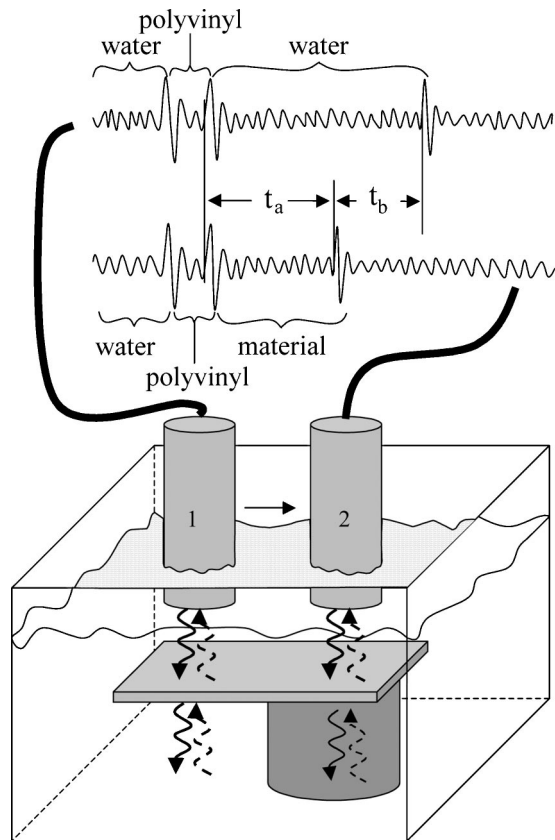


FIG. 6. Experimental set-up used to measure the acoustic velocity of the agar–oil gel (identified as the material on the figure). Because the acoustic impedance of agar gel is close to that of water filling the reservoir, a thin plate of polyvinyl was inserted on the top of the agar tissue sample to produce acoustic impedance mismatches and thus to help identify the frontiers of the different echoes.

literature.⁷ However, since this can have an impact on the accurate 3-D registration of the fiducial markers, the acoustic velocity of the agar–oil gel forming the first layer of the phantom was measured using a pulse transit time technique similar to that described by Madsen *et al.*²³ The experimental setup is shown in Fig. 6. The distance from the transducer to fixed targets located in a water bath was measured with a pulser/receiver (Panametrics, Waltham, MA, #5900 PR) from the 10 MHz radio-frequency signal digitized with a Gage 8500 PC card (Gagescope, Montreal, Canada). A 40- μ s duration ultrasound pulse was transmitted through a known thickness of tissue-mimic and the speed of sound c was measured according to the following equation: $c_{\text{agar-oil}} = c_{\text{water}} \times (t_a + t_b) / t_a$, where c_{water} is the speed of sound in water at room temperature (1480 m/s), t_a , shown in Fig. 6, is the propagation time in the block of agar–oil, and t_b is the propagation time difference for the echo to reach the bottom of the water tank in the presence or absence of the agar–oil block of material. The measurement was repeated for three different samples with different concentrations of paraffin oil in the agar gel (0%, 33% and 100%) at room temperature (22 °C). As described earlier, the concentration of 100%, for example, was obtained by mixing an equivalent volume of agar gel and paraffin. To validate our method, the same ex-

perimental approach was also used to measure the speed of sound in standard agar gel, and a comparison was made with the literature.⁷

E. Geometric assessments of the vessel lumen diameter

For each step involved in manufacturing the vascular phantom, several factors could affect the geometric accuracy of the lumen. One major advantage of the current phantom is the possibility of using the computer assisted design (CAD) file, used to fabricate the mold of the vessel lumen, as the 3-D geometric gold standard for the calibration of the multimodality imaging methods. Therefore, it was mandatory to validate the different steps of the fabrication process.

1. Molding of cerrowal

The geometric accuracy following the molding of cerrowal was first tested by comparing the inner 7.9 mm diameter of the aluminum mold to the diameter of a cerrowal rod casted in it. The cerrowal bar was prepared according to the method described earlier. At three different positions along the bar, the diameter was measured five times by using a microcaliper following rotation of the rod. The diameters obtained ($n = 15$) were then compared to the theoretical measure of the mold.

2. Heating the phantom

In order to evaluate the impact of heating cerrowal on the agar–gel structural stability, two phantoms were made using a 7.9 mm diameter stainless steel rod instead of cerrowal to produce the lumen inside the gel. After removing the rod by sliding it through the garolite inlets, one model was cut perpendicularly into ten thin slices of 200 μ m with a microtome, while the other model was heated at 65 °C in water for two hours, cooled down to the ambient temperature and cut according to the same procedure. The lumen diameter of each film was measured at five different angles with a Leica microscope. The measures of the control ($n = 50$) and heated ($n = 50$) models were then compared.

3. Pressurizing the vessel lumen

Two agar–gel models surrounding a cerrowal stick of 7.9 mm diameter covered with latex were prepared. The agar–gel models were heated at 65 °C to melt the cerrowal and to produce the lumen within the phantom. The lumen of each of them was then filled with an agar–gel at a pressure of 20 and 100 mm Hg, respectively. The pressure was maintained until the gel hardened. Each model was then cut perpendicularly into either six (20 mm Hg) or five (100 mm Hg) thin slices of 200 μ m with a microtome, and the diameter of the gel cylinder inside the latex wall was measured at five different angles with the Leica microscope. The diameters of the agar rod ($n = 30$ or 25) were then compared with the measures made on the cerrowal stick to evaluate the need of pressuring the vessel to stretch out the latex layer. This may be necessary for an accurate calibration of radiographic imagers since latex and agar gel do not bind together.

4. Possible degradation over time

Finally, in order to evaluate the impact of storage on the geometric accuracy of the agar gel, another model was constructed with a stainless steel rod of 7.9 mm diameter. To maintain consistency, although it was not necessary for the removal of the rod, the model was heated in water at 65 °C for two hours. Then, the agar block was removed from the phantom and a portion of it was cut perpendicularly into five thin slices of 200 μm with a microtome, while the other part was conserved for 30 months in a solution of water and sodium azide (0.1%, Sigma Chemical, St. Louis, MO, #S2002) at 4 °C. The addition of sodium azide to the water allowed us to eliminate the bacterial proliferation. After 30 months, the second part of the agar block was also cut into five thin slices. The tube diameter of each slice was measured at five different angles for each block with the Leica microscope, and the values ($n=25$) were compared.

F. Image acquisitions

All image acquisitions were performed by using standard clinical protocols. DSA projections were acquired on a DFP 2000 unit (Toshiba, Tokyo, Japan) by using the following parameters (field-of-view=17 cm, tube-intensifier distance=100 cm, table height=80 cm, matrix size=1024 \times 1024, current density=400 mA and peak voltage=70 kV). The vascular phantom was filled with a contrast solution of iohalamate meglumine at 300 mg/ml (Conray 30, Mallinckrodt Medical, Pointe-Claire, QC, Canada). For the CT-scans, the vessel lumen was filled with a 2.8% solution of 430 mg/ml of iohalamate meglumine (Conray 43) diluted in a 0.9% NaCl solution. The phantom was scanned with a PQ5000 scanner (Philips Medical System, Best, The Netherlands) by using a slice thickness of 1 mm, a pitch of 1.25 mm and a reconstruction interval of 1 mm. Other parameters for all CTA scans were a current density of 200 mA, a peak voltage of 120 kV, a matrix size of 512 \times 512, and a field of view of 25 cm. An ATL Ultramark 9 HDI ultrasound system (Philips Medical System, Bothell, WA, USA) with a 38-mm aperture linear array probe (L7-4) was used to collect B-mode images at 5 MHz. The focal point of the ultrasound beam was set near the center of the vessel lumen filled with distilled water. A 3-D imaging system (Life Imaging, London, ON, Canada) was used for the B-mode image acquisition and display. A discrete movement step motor was used to longitudinally scan the phantom at a slow velocity of 0.25 mm/s. The 2-D cross-sectional images had a dimension of 256 \times 256 pixels. Magnetic resonance imaging was performed with a 1.5 Tesla unit (Magnetom Vision, Siemens, Erlangen, Germany). The phantom vessel was filled with a 1.8 millimole/L of gadopentetate dimeglumine solution ("gadolinium," Magnevist, Berlex, Lachine, QC, Canada) diluted in a 0.9% NaCl solution. A high resolution three-dimensional fast low angle shot (FLASH) sequence in the coronal plane using a body array coil was used (repetition time=4.6 ms, echo time=1.8 ms, flip angle=30°, field of view=293

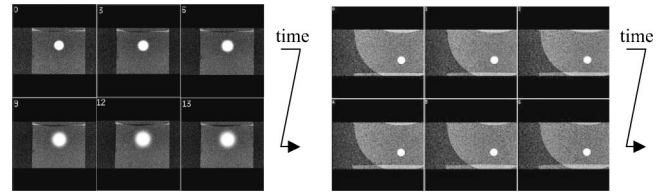


FIG. 7. MRA cross-sectional images of the phantom without (left panel) and with (right panel) the use of a latex membrane to simulate the vessel wall. The diffusion testing of gadolinium was performed over a period of 5 hours.

$\times 390$ mm, matrix size=194 \times 512, slab thickness=60 mm, effective slice thickness=1.67 mm, 50% overlap, number excitation=1).

III. RESULTS

A. Effectiveness of the latex membrane to prevent diffusion of contrast agent

The possible diffusion of gadolinium through the vessel wall was tested in MRA. Figure 7 shows 5 hours testing without and with the latex membrane. As seen on the left panel, important diffusion within the agar gel was noted when the phantom was constructed without spraying the cerulow bar with latex. On the contrary, the use of the latex barrier avoided diffusion. For instance, no significant change in the vessel cross-sectional area was noted over the observation period of 5 hours. In the current study, no diffusion testing was performed with x-ray iodine contrast or ultrasound bubbles. Because of the latex barrier, no diffusion for both contrast agents are expected.

B. Tissue-mimic ultrasound properties

As described in Sec. II, two compounds were used to create the first and second semi-cylindrical layers of agar-based gels. In the first layer that includes the fiducial markers, the gel was made of 3 weight percent of agar and 97 weight percent of water to which 33% in volume of paraffin oil was added. According to Table I, the speed of sound in this compound was 1485 ± 0.9 m/s, which is lower than the speed of sound in biological tissues (1540 m/s). As a reference, the velocities for other volume concentrations of paraffinic oil are also given. The sound velocity in the agar gel of the second layer (3% agar, 8% glycerol, 3% cellulose and 86% water) was 1545 ± 1.1 m/s, as expected.⁷

TABLE I. Acoustic properties of agar-gel with a different concentration of paraffin oil at 22 °C (mean \pm standard deviation).

% of paraffin oil	Speed (m/s)
0%	1500 \pm 1.5
33%	1485 \pm 0.9
100%	1469 \pm 0.9

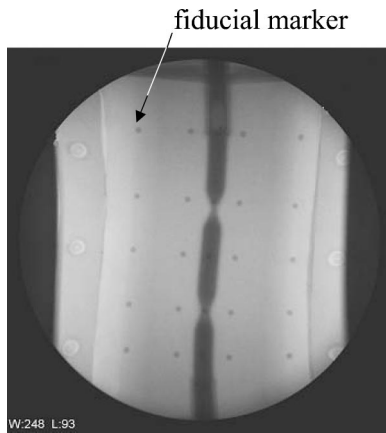


FIG. 8. Lateral angulation view of the phantom imaged on a digital subtraction angiography scanner. Twenty of the twenty-five fiducial markers are clearly visible on this scan projection. The other five markers are underneath the stenosed vessel.

C. Geometric measurements of the vessel lumen diameter

The geometric accuracy following the molding of a 7.9 mm diameter cerrow bar was tested by comparing the averaged diameter of the cerrow stick with that of the aluminum mold. The agreement was within -0.5% (-0.04 ± 0.06 mm), which is satisfying (the slight hand polishing of the cerrow bar following its removal from the mold may partially explain this difference). The geometry of the mold or that of the CAD file can thus be considered as the gold standard lumen diameter of the phantom (if high precisions are assured during the fabrication of the mold). In addition, it appears that heating the model in water at 65°C for 2 hours had no effect on the geometric accuracy of the agar-gel. The diameter difference between the stainless steel rod and that of the sliced lumens measured with a microscope, following heating (-0.11 ± 0.07 mm) or not (-0.10 ± 0.07 mm) of the gel was similar ($p=0.44$, t -test) and within -1.4% of the true diameter of the rod.

The need of pressurizing the lumen to extend the latex layer has been tested by comparing the theoretical diameter of 7.9 mm to the average diameter of two lumens filled with an agar gel at 20 and 100 mm Hg, respectively. The results showed that at 100 mm Hg of pressure, the average diameter differences of the gel cylinder inside the latex layer were similar to the desired geometry (-0.004 ± 0.18 mm), while a slight difference (-0.20 ± 0.30 mm, -2.5% , $p=0.006$, t -test) was noted for the model filled with agar at 20 mm Hg. Finally, it appeared that the agar-gel slightly shrunk over the storage period of 30 months (-0.26 ± 0.08 mm, -3.3% , $p < 0.001$, t -test).

D. Visualization of the phantom with the multimodality radiographic imagers

Figure 8 presents a DSA image plane obtained from a lateral angulation view, whereas a CTA cross-section of the same vascular phantom is shown in Fig. 9. The pincushion distortion of the angiographic scanner is clearly visible in

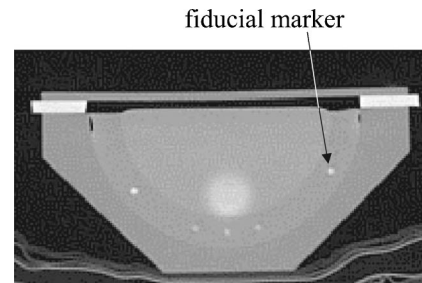


FIG. 9. A cross-sectional view of the phantom imaged on a digital computerized tomography scanner. Five fiducial markers are clearly seen on this image section.

Fig. 8. Figures 10 and 11 show the phantom imaged with B-mode ultrasound and MRA, respectively. For all imaging modalities, the lumen with double stenoses and fiducial markers were clearly identifiable without a significant artifact.

IV. DISCUSSION

The components and proportions of the agar and agar-oil gel mixtures, as well as the fiducial markers, had to be chosen so that they met two major requirements: first, materials

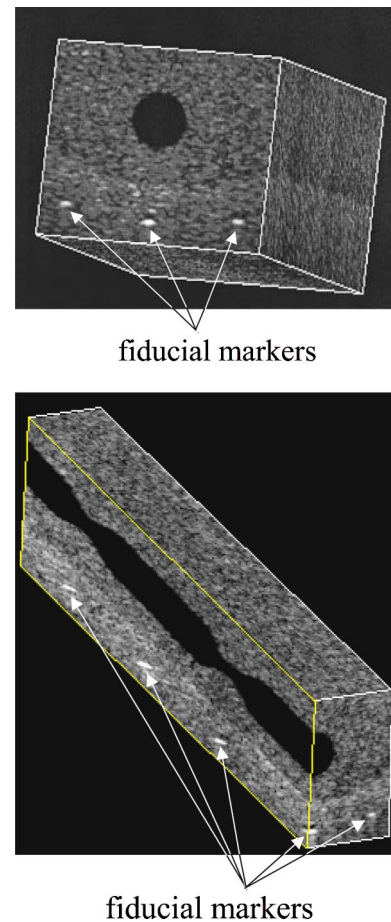


FIG. 10. 3-D volumes of the phantom imaged with a B-mode ultrasound scanner. The fiducial markers aligned with the plane views selected were clearly visible.

fiducial marker

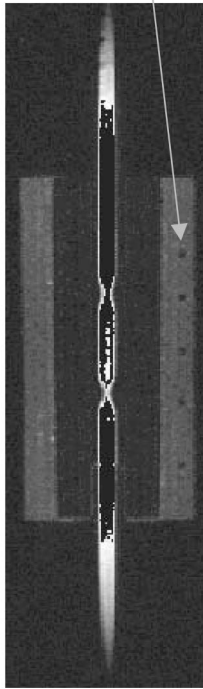


FIG. 11. A horizontal section view of the phantom visualized on a magnetic resonance imaging scanner. A row of five fiducial markers is clearly visible in hypo-signal; the other twenty markers are not seen on this 2-D plane view. Since the window width setting to visualize the markers was narrow, the signal intensity in the lumen appears saturated.

used to manufacture the phantom had to create no or minimum artifacts on images in any modality; and second, the markers had to be easily detected and identified. Markers appear clearly on phantom images if there is high contrast between them and the material in which they are inserted. It was strategically decided to use solid markers to prevent the risks of diffusion into the surrounding agar gel, which could happen if one had chosen to use liquid markers consisting of a fluid embedded in sealed cavities (e.g., encapsulated MRA contrast agents such as gadolinium, or any other materials).²¹

Using the fabrication techniques presented here, sophisticated multimodality anthropomorphic phantoms of known geometries are possible. The ability to create many exact duplicates of the model permits investigators to perform simultaneous experiments on identical models at different sites or at different moments. Moreover, one phantom may be used for repeated experiments system calibration and quality assurance applications. If a phantom should become damaged or lost it can be easily replaced since identical casts may be made from the mold.

A. Rationale for the selection of glass markers embedded in an agar–oil mixture gel

For imaging techniques based on x-ray (DSA, CTA), contrast on the images results from a difference in x-ray absorption of the different materials. Consequently, materials like glass, which have an absorption coefficient significantly higher than that of agar–gel⁶ (around 0.24 cm^{-1} for agar–

gel versus $1 \text{ to } 10 \text{ cm}^{-1}$ for different kinds of glasses, at 90 kVp), will appear clearly both in DSA and CTA images, as it can be seen in Figs. 8 and 9. In acoustic imaging, the contrast between two adjacent materials results from a difference in acoustic impedance. Agar gels are known to have an acoustic impedance of about $1.5 \times 10^5 \text{ g/cm}^{-2} \text{ s}^{-1}$ (see Ref. 6). For a mixture of agar gel with oil, the acoustic impedance is slightly lower according to Table I (the acoustic impedance is proportional to the sound velocity). Therefore, as far as acoustic imaging is concerned, fiducial markers could be made of any materials having a much (for example ten times) greater impedance, for them to be clearly seen. On the other hand, the material of the fiducial markers should not have a too high mismatch in acoustic impedance to avoid exaggerated attenuation and shadowing behind the markers. In the specific example described in the present study, glass balls (impedance of $14 \times 10^5 \text{ g/cm}^{-2} \text{ s}^{-1}$; see Ref. 24) were used as markers. They appeared as white bright spots on B-mode ultrasound images (see Fig. 10). For MRA, contrast is essentially based on the difference in relaxation times (longitudinal relaxation time T_1 and transverse relaxation time T_2). MRA sequences are usually T_1 -weighted because they are performed after gadolinium bolus injection inducing a shortening of blood T_1 value. As the recovered spin-echo signal is a decreasing function of T_1 , materials with short longitudinal relaxation time appear bright on T_1 -weighted images. In the current study, metallic markers could not be used because they create artifacts that prevent a precise determination of the center of the markers on images. Small glass balls were used instead because they are compatible with MRA in addition to being a good selection for ultrasound and x-ray. Since the T_1 of agar gel is low,⁶ and not very different from that of glass (T_1 around 1000–1200 ms), glass markers cannot easily be detected when inserted in agar–gel alone. As fat components (e.g., adipose tissues on medical images²⁵) are known to have shorter values of T_1 (around 200–500 ms), it was decided to add oil into the agar-based gel layer in which markers were inserted. The signal level of the agar–oil gel mixture was then much higher, and the fiducial glass markers thus appeared as black spheres (hypo-signal) on a light-gray background, as can be seen in Fig. 11.

B. Other technical considerations

As agar-based gels contain a great amount of water, mixing them with a high proportion of oil or fat component can be difficult (problems of homogeneity of the mixture resulting in the apparition of oil bubbles inside the gel matrix), and, with excessive oil concentration, the resulting mixture may not be able to harden. For this reason, although high oil concentrations provide better contrast with glass markers, the proportion of oil included in the preparation of the gel was selected to be in the range of 30%–50% in volume (33% in the examples presented here). This was found to be a good compromise between contrast, homogeneity of the mixture and hardening.

Degradation of the latex membrane mimicking the vessel

wall was observed over time. This seemed to be due to the absence of a dry barrier between latex and the agar gel (made of 86% water) surrounding the vessel. To circumvent this problem, a thin layer of polyurethane was recently added over the latex membrane before introducing the cerrolow bar within the phantom. This strategy seems to provide a solution for this problem and it is expected to increase the long-term durability of the phantom. Polyurethane may also be advantageous in future developments to avoid the need of pressurizing the lumen at 100 mm Hg for an accurate assessment of its dimension. For instance, latex binds to the stiffer polyurethane membrane and it may thus be possible to use the phantom at the atmospheric pressure if this solution proves successful.

We are aware that the use of latex alone may also be problematic if one considers flow experiments. For instance, the pressure drop downstream of a stenosis may create pulsatile oscillations of the latex membrane under physiological flow conditions. The addition of polyurethane may be beneficial for this potential problem because latex would no longer move away of the agar gel. Finally, it is important to mention that the inner surface of the vessel wall should be made of latex instead of polyurethane alone because this facilitates the removal of residual cerrolow particles following heating at 65 °C.

Two additional aspects need to be discussed here: the first one is related to the possible geometric distortion in US scans, and the other concerns the long-term geometrical stability of the phantom. As reported in Table I, the acoustic velocity of the agar–oil mixture (33%) slightly differed from that of the agar gel forming the core of the phantom. Consequently, misregistration in the 3-D positioning of the fiducial markers can theoretically occur. If one considers the dimension of the phantom and an ultrasound probe scanning the vessel perpendicularly, the range of errors in the estimate of the distances between the top of the agar gel filling the phantom and the fiducial markers is between 0.4–1.3%, which is negligible (for the glass balls below the vessel, the ultrasound beam propagates back and forth in 40 mm of agar and 4.5 mm of agar–oil, whereas for the balls closest to the top surface, the distances are 16 mm in agar and 9.3 mm in agar–oil). In addition, it is important to note that the 7-mm thick polyethylene sheet covering the phantom does not induce 3-D echographic distortion. However, a constant vertical shift in the actual position of the vessel lumen and fiducial markers does occur (a shift of -1.9 mm, considering a speed of sound in low density polyethylene of 1950 m/s; see Ref. 24). Finally, as reported earlier, a slight reduction in the vessel lumen diameter (-3.3%) was noted over a period of 30 months. This may be attributed to the storage condition. The long-term stability of the vessel lumen dimension may need additional validation, although it is expected that much better results would have been obtained if the agar gel surrounding the vessel had been sealed in the vascular phantom during storage.

V. CONCLUSION

In this article, the process for manufacturing a novel multimodality vascular imaging phantom was presented. Fiducial markers embedded in the structure of the phantom were clearly identifiable on each radiographic imaging modality tested (digital subtraction angiography, computerized tomography angiography, B-mode echography and magnetic resonance angiography). The phantom was recently validated as a tool for the calibration of multimodality images of cylindrical vessel sizes ranging between 0.93 and 6.24 mm.²⁶ It was also used to optimize peripheral MRA acquisition parameters for the purpose of quantifying peripheral vascular stenoses.²⁷ Finally, a nitinol stent with tantalum markers was recently implanted in the structure of the vascular phantom to evaluate artifacts produced on MRA and CTA imaging.²⁸

ACKNOWLEDGMENTS

The authors acknowledge the contribution of Mr. Michel Daronat for measuring the acoustic velocity in the agar–oil mixture, and Mrs. Richard Cimon and Damien Garcia for their technical advice and help during the development and testing of the phantom. This work was supported by grants from the Canadian Institute of Health Research (GC, LGD, GS, #MOP-53244) and Valorisation-Recherche Québec (group Grant No. 2200-094), and by research scholarship awards from the Fonds de la Recherche en Santé du Québec (G.C. and G.S.).

^{a)}Send correspondence to Dr. Guy Cloutier, Director, Laboratory of Biorheology and Medical Ultrasonics, Research Center, Centre hospitalier de l'Université de Montréal, 2099 Alexandre de Sève (room Y-1619), Montréal, Québec H2L 2W5, Canada. Electronic mail: guy.cloutier@umontreal.ca

^{b)}Dr. S. D. Qanadli is now with the Department of Radiology, University of Lausanne–CHUV, Lausanne, Switzerland.

¹J. V. Hajnal, D. L. G. Hill, and D. J. Hawkes, *Medical Image Registration*, edited by M. R. Neuman (CRC, Boca Raton, 2001).

²K. F. Kreitner, P. Kalden, A. Neufang, C. Duber, F. Krummenauer, E. Kustner, G. Laub, and M. Thelen, "Diabetes and peripheral arterial occlusive disease: Prospective comparison of contrast-enhanced three-dimensional MR angiography with conventional digital subtraction angiography," *Am. J. Roentgenol.* **174**, 171–179 (2000).

³J. T. Bushberg, J. A. Seibert, E. M. Leidholdt, Jr., and J. M. Boone, *The Essential Physics of Medical Imaging*, 2nd ed. (Lippincott Williams & Wilkins, Philadelphia, 2002).

⁴W. N. McDicken, *Diagnostic Ultrasonics: Principles and Use of Instruments*, 3rd ed. (Churchill Livingstone, Edinburgh, 1991).

⁵M. M. Burlaw, E. Madsen, J. A. Zagzebski, R. A. Banjavic, and S. W. Sum, "A new ultrasound tissue-equivalent material," *Radiology* **134**, 517–520 (1980).

⁶R. Frayne, L. M. Gowman, D. W. Rickey, D. W. Holdsworth, P. A. Picot, M. Drangova, K. C. Chu, C. B. Caldwell, A. Fenster, and B. K. Rutt, "A geometrically accurate vascular phantom for comparative studies of x-ray, ultrasound, and magnetic resonance vascular imaging: Construction and geometrical verification," *Med. Phys.* **20**(2), 415–425 (1993).

⁷D. W. Rickey, P. A. Picot, D. A. Christopher, and A. Fenster, "A wall-less vessel phantom for Doppler ultrasound studies," *Ultrasound Med. Biol.* **21**, 1163–1176 (1995).

⁸Z. Guo and A. Fenster, "Three-dimensional power Doppler imaging: A phantom study to quantify vessel stenosis," *Ultrasound Med. Biol.* **22**, 1059–1069 (1996).

- ⁹F. Dong, E. L. Madsen, M. C. MacDonald, and J. A. Zagzebski, "Non-linearity parameter for tissue-mimicking materials," *Ultrasound Med. Biol.* **25**, 831–838 (1999).
- ¹⁰J. Wu, "Tofu as a tissue-mimicking material," *Ultrasound Med. Biol.* **27**, 1297–1300 (2001).
- ¹¹C. P. Renaudin, B. Barbier, R. Roriz, D. Revel, and M. Amiel, "Coronary arteries: new design for three-dimensional arterial phantoms," *Radiology* **190**, 579–582 (1994).
- ¹²K. Bendib, C. Poirier, P. Croisille, J. P. Roux, D. Revel, and M. Amiel, "Caractérisation d'une sténose artérielle par imagerie 3D. Comparaison, grâce à des fantômes physiques, de 3 techniques d'acquisition (ARM, TDMH, ARX 3D) et de 4 modalités de visualisation (MIP, SR, MPVR, VA)," *J. Radiol.* **80**, 1561–1567 (1999).
- ¹³R. Fahrig, H. Nikolov, A. J. Fox, and D. W. Holdsworth, "A three-dimensional cerebrovascular flow phantom," *Med. Phys.* **26**, 1589–1599 (1999).
- ¹⁴E. Berry, A. Marsden, K. W. Dalgarno, D. Kessel, and D. J. A. Scott, "Flexible tubular replicas of abdominal aortic aneurysms," *Proc. Inst. Mech. Eng., Part H: J. Eng. Med.* **216**, 211–214 (2002).
- ¹⁵R. V. Yedavalli, F. Loth, A. Yardimci, W. F. Pritchard, J. N. Oshinski, L. Sadler, F. Charbel, and N. Alperin, "Construction of a physical model of the human carotid artery based upon *in vivo* magnetic resonance images," *Trans. ASME, J. Biomech. Eng.* **123**, 372–376 (2001).
- ¹⁶C. W. Kerber and C. B. Heilman, "Flow dynamics in the human carotid artery: I. Preliminary observations using a transparent elastic model," *Am. J. Neuro.* **13**, 173–180 (1992).
- ¹⁷W. Dabrowski, J. Dunmore-Buyze, R. N. Rankin, D. W. Holdsworth, and A. Fenster, "A real vessel phantom for imaging experimentation," *Med. Phys.* **24**, 687–693 (1997).
- ¹⁸W. Dabrowski, J. Dunmore-Buyze, H. N. Cardinal, and A. Fenster, "A real vessel phantom for flow imaging: 3-D Doppler ultrasound of steady flow," *Ultrasound Med. Biol.* **27**, 135–141 (2001).
- ¹⁹J. L. Creasy, D. B. Crump, K. Knox, C. W. Kerber, and R. R. Price, "Design and evaluation of a flow phantom," *Acad. Radiol.* **2**, 902–904 (1995).
- ²⁰R. F. Smith, B. K. Rutt, and D. W. Holdsworth, "Anthropomorphic carotid bifurcation phantom for MRA applications," *J. Magn. Reson. Imag.* **10**, 533–544 (1999).
- ²¹D. L. G. Hill, "Combination of 3-D medical images from multiple modalities," thesis submitted for the degree of doctor of philosophy, University of London, United Kingdom, 1993.
- ²²M. J. Gordon, K. C. Chu, A. Margaritis, A. J. Martin, C. R. Ethier, and B. K. Rutt, "Measurement of Gd-DTPA diffusion through PVA hydrogel using a novel magnetic resonance imaging method," *Biotechnol. Bioeng.* **65**, 459–467 (1999).
- ²³E. L. Madsen, F. Dong, G. R. Frank, B. S. Garra, K. A. Wear, T. Wilson, J. A. Zagzebski, H. L. Miller, K. K. Shung, S. H. Wang, E. J. Feleppa, T. Liu, W. D. O'Brien, Jr., K. A. Topp, N. T. Sanghvi, A. V. Zaitsev, T. J. Hall, J. B. Fowlkes, O. D. Kripfgans, and J. G. Miller, "Interlaboratory comparison of ultrasonic backscatter, attenuation, and speed measurements," *J. Ultrasound Med.* **18**, 615–631 (1999).
- ²⁴A. R. Selfridge, "Approximate material properties in isotropic materials," *IEEE Trans. Sonics Ultrason.* **SU-32**, 381–394 (1985).
- ²⁵P. A. Bottomley, T. H. Foster, R. E. Argersinger, and L. M. Pfeifer, "A review of normal tissue hydrogen NMR relaxation times and relaxation mechanisms: Dependence on tissue type, NMR frequency, temperature, species, excision, and age," *Med. Phys.* **11**, 425–448 (1984).
- ²⁶N. Boussion, G. Soulez, J. de Guise, M. Daronat, Z. Qin, and G. Cloutier, "Geometrical accuracy and fusion of multimodal vascular images: A phantom study," *Med. Phys.* **31**, 1434–1443 (2004).
- ²⁷A. Tang, G. Soulez, G. Beaudoin, S. Qanadli, E. Thérèse, and G. Cloutier, "Optimization of peripheral MRA acquisition parameters: a vascular phantom study," Annual Meeting of the Society of Interventional Radiology, April 2003.
- ²⁸L. Létourneau-Guillon, G. Soulez, G. Beaudoin, V. L. Oliva, M. F. Giroux, Z. Qin, N. Boussion, E. Thérèse, J. de Guise, and G. Cloutier, "CT and MR imaging of nitinol stent with radio-opaque distal markers," *J. Vasc. Interv. Radiol.* (in press).